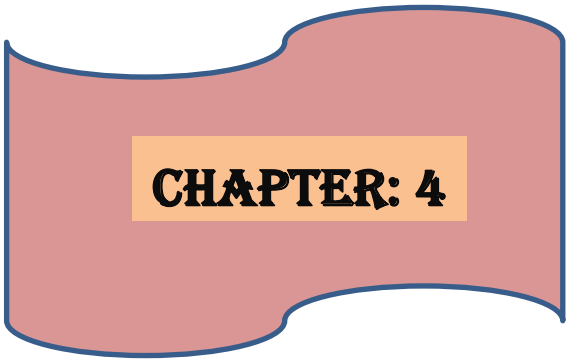

Space Charge Layer Induced Superionic Conduction and Charge Transport Behaviour of "Alkali Carbonates and tri-doped Ceria Nanocomposites" for LT-SOFCs Applications

4.1 Introduction

As discussed in Chapter I, solid electrolytes having high oxide ion conduction with low operating temperature are the main requirements for the commercialization of SOFCs. The reduced conductivity of Yttrium stabilized zirconia (YSZ) at lower operating temperatures cannot meet this requirement. Gadolinium doped ceria (GDC) and Samarium doped ceria (SDC) were developed to overcome the limitations of YSZ as they present considerably higher oxygen ion conductivity at comparatively lower working temperatures (500-700°C). In doped ceria, the oxide ion conductivity generally depends upon the concentration and nature of dopant ions, free oxygen vacancies, mobile charge ions, local defect structure, and migration energy of ions etc. When a trivalent rare earth ion is doped in a CeO_2 lattice, oxygen ion conduction is facilitated by formation and migration of free oxide ions through oxygen vacancies via charge compensation mechanism. Therefore, to achieve the higher oxide ion conductivity, electrolytes having high accessibility of oxygen vacancies, is a key factor [Yang et al., 2013; Yang et al., 2014; Anirban et al., 2016]. In view of this, with the aim of utilizing rare earth ions to develop doped and co-doped ceria electrolyte materials, many researchers have investigated electrolytes such as $Sm_xNd_{0.15-x}Ce_{0.85}O_{2-\delta}$ [Rai et al., 2014], $Ce_{1-a}Gd_{a-y}Sm_yO_{2-0.5}$ [Wang et al., 2004], $Ce_{1-x}Ho_{0.1}Sr_xO_{2-\delta}$ [Anirban et al., 2018], $Ce_{1-x}(Y_{0.5}Dy_{0.5})_xO_{2-\delta}$ [Tadokoro et al., 2007], $Ce_{1-x}(Gd_{0.5}Pr_{0.5})_xO_{2-\delta}$ [Ramesh et al., 2012], $Gd_{0.2-x}Dy_xCe_{0.8}O_{1.9}$ [Khakpour et al., 2014], $Ce_{0.8}Sm_{0.2-x}Pr_xO_{2-\delta}$ [Lin et al., 2015], $Ce_{0.7}Pr_{0.15}Sm_{0.075}Eu_{0.075}O_2$ [Anirban et al., 2016] etc. Major drawbacks linked with the use of doped ceria materials as solid electrolytes are the tendency of rising electronic conductivity due to altering the valence state from Ce^{4+} to Ce^{3+} in the reducing environment, and segregation of impurities resulting into extremely resistive layer at the grain boundaries. The co-doping or multiple cations doping approach show

the ways to solve this problem and improve the properties of electrolyte materials. However, the occurrence of impurities (such as silica) and formation of space charge layer (SCL) which deplete the pathway of oxygen vacancies along the grain boundaries offers significant resistance along the grain boundary, deteriorating the response. Thus, considerable interest should be given to the characteristics of grain boundaries along with the grains to develop a suitable material for low/intermediate temperature electrolyte. Several studies revealed that co-doping approach is useful to get better conductivity of electrolyte simply at intermediate temperature range at optimum concentration of dopants [Omar et al., 2006; Anwar et al., 2018; Accardo et al., 2018; Zagaynov et al., 2017; Daza et al., 2018]. Moreover, many novel approaches have been considered in recent years, aiming to explore new electrolyte materials with desirable performance at relatively low operating temperatures. In this context, doped ceria-Alkali carbonates nanocomposite electrolyte is observed to exhibit most promising performance at lower as well as intermediate temperature ranges. These nano composites utilize the novel approach of having molten carbonates (amorphous phase) incorporated and uniformaly distributed in the interfacial regions of doped ceria grains [Ali et al., 2013; Zhu et al., 2001; Ristoiu et al., 2012]. The large molten carbonate interfacial regions in the grain boundary areas leads to promote the amount of free charge defects in space charge regions and provide superionic conduction between two constituent phases. In view of these features, a series of well-designed doped ceria-alkali carbonates two-phase based nanocomposite materials have been investigated in last few years to improve the oxygen ionic conductivity, power efficiency and performance of fuel cells having doped or co-doped ceria based SOFCs electrolytes which could work in the low as well as intermediate temperature regions [Jaiswal et al., 2015; Jaiswal et al., 2015; Raza et al., 2020].

In a previous work on tri-doped ceria, Venkataramana et al. [Venkataramana et al., 2017] have reported that the composition $Ce_{0.76}Pr_{0.08}Sm_{0.08}Gd_{0.08}O_{2-\delta}$(CPSG) shows optimum ionic conductivity (1.86×10^{-2} S-Cm^{-1}) at 600°C with less activation energy (0.56eV), which makes it suitable as a good electrolyte material for SOFCs. Thus, it can be a potential material for developing nanocomposites with lithium/sodium carbonates having better performance as electrolyte material at low and intermediate operating temperatures. In view of this, we have prepared several compositions of Pr-Sm-Gd tridoped ceria/lithium-sodium carbonates (CPSG/LNC) nanocomposites and optimized the composition for best response of electrolyte at lower operating temperatures. The central plan of this effort is to explore the outcome of addition of binary LNC carbonates on the crystal structure, morphology, ionic conductivity and charge transport properties in CPSG/LNC nanocomposites. The results presented in this chapter reveal, the existence of superionic conduction via induced space charge layer and multi-ions conduction along composite interfaces.

4.2 Experimental details

4.2.1 Synthesis of samples

The $Ce_{0.76}Pr_{0.08}Sm_{0.08}Gd_{0.08}O_{2-\delta}$ (CPSG) nanocrystalline ceramic powder was synthesized by glycine auto combustion synthesis method as described in detail in chapter 2. In the preparation procedure, stoichiometric quantities of CeO_2, Pr_6O_{11}, $Sm(NO_3)_3$, $Gd(NO_3)_3$ were used as reactant and glycine as a fuel. The binary mixture of lithium carbonate and sodium carbonate containing molar ratio 52/48 was mixed separately by using conventional solid-state ceramic route. $Ce_{0.76}Pr_{0.08}Sm_{0.08}Gd_{0.08}O_{2-\delta}$ powder and eutectic binary mixture of $(Li_{0.52}\text{-}Na_{0.48})_2CO_3$ (LNC) was grounded thoroughly in agate motor with various composite compositions in weight fractions of 80/20, 70/30 and 65/35 abbreviated as CPSG/20LNC, CPSG/30LNC and CPSG/35LNC

respectively. Mixed powders of various compositions were dried for 24 h at 100 °C in an electric oven followed by calcination in air for 600°C for 2 h. The obtained powders were pelletized into uniform circular pellets (thickness ~1 mm, diameter ~10mm) under 50 kN of optimized load using a hydraulic press. These composite pellets were sintered in muffle furnace for densification in air at 700 °C for 1.5 h. In case of CPSG, the sintering was carried out in SiC furnace at 1300°C for 4 h.

4.2.2 Characterizations

Phase identification of pure phase and composite electrolyte samples were done by Rigaku Miniflex 600 powder X-ray diffractometer with CuK_{α} (λ=1.5406Å) radiation by recording data over a 2θ range (20°-100°) with step width of 0.02°. The lattice parameters and average crystallite size of all the samples were determined by Rietveld structure refinement and Scherrer's formula, respectively. Thermal characteristics of as synthesized samples were studied by using Differential Thermal analysis (DTA) analysis (Mettler Toledo) from room temperature (RT) to 800°C in N_2 environment. The microstructure and morphology of surface of pellets were observed via scanning electron microscope by using ZEISS EVO 18. For impedance analysis, silver paste were used to make electrode on both flat sides of pellets and cured for 15 min at 500°C. Transmission electron microscopy for characterizing the crystal structure and microstructure was done using Tecnai G220 TWIN. A KEYSIGHT-E4990A, impedance analyzer was carried out to record the impedance data of sintered pellets of various compositions over the frequency range (20Hz -5MHz) from 300 to 650°C temperature range in static ambient atmosphere. To find out the ionic conductivity of solid electrolytes, as a result of contribution of resistance along the grain boundary and grain resistance, Zsimpwin software was applied to fit the response data from impedance analyzer in equivalent electric circuits. A Rigaku Smart Lab 9kW Powder

diffractometer having high temperature X-ray diffraction (HT-XRD) attachment was used to perform high temperature XRD measurements. The structural parameters determined by Rietveld structure refinement from HT-XRD data were employed to determine the thermal expansion of composite samples in the temperature range 30 to 700°C.

4.3 Results and Discussion

4.3.1 Thermal Analysis

The typical DTA plots over the temperature range of RT to 800 °C, for the as-prepared CPSG and CPSG/LNC composite powders obtained after auto combustion, are presented in Figure 4.1. Thermal behavior of pure CPSG sample shows only one broad endothermic peak attributed to crystallization of pure sample during thermal treatment whereas, the CPSG/carbonates composites exhibit two endothermic peaks at two different temperatures. The initial peak around 100 °C is attributed to the vaporization of adsorbed surface water and the next peak around ~ 500°C appears due to the eutectic transition point melting of LNC and formation of a molten form of binary alkali carbonate salt [Ali et al., 2018]. It can also be seen that peak of eutectic point of composites shift in the direction of higher temperature with increasing the content of alkali carbonates. The same trend was also revealed in earlier reported works [Anjaneya et al., 2013; Kosinski et al., 2011]. The amorphous character of mixed alkali carbonates phase on the CPSG surface facilitates extra path for ions transport at an elevated temperature. The mixed alkali carbonates also show amorphous softening nature, which suppresses the electronic conductivity and improves ionic conduction through extra pathway for ion transport [Anjaneya et al., 2013]. The DTA curves shown in Figure 4.1 also confirm that there is no chemical reaction between tri-doped ceria CPSG, and carbonates phases.

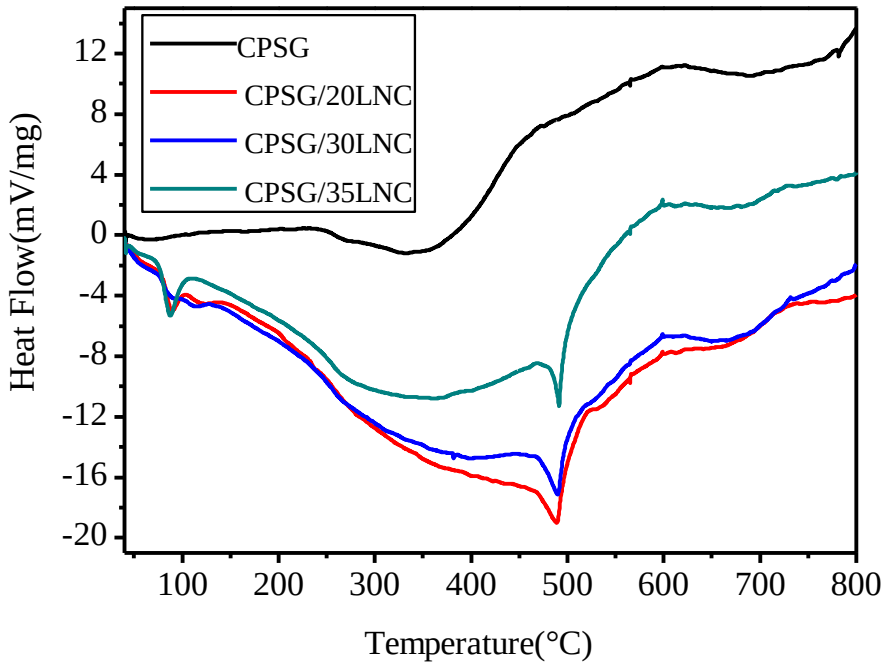

Figure 4.1 DTA profiles of the CPSG, CPSG/20LNC, CPSG/30LNC and CPSG/35LNC nanocomposite electrolytes.

4.3.2 X-ray diffraction studies

Powder X-ray diffraction profiles of various compositions of the nanocomposites obtained after sintering are shown in Figure 4.2. The major diffraction peaks in the XRD profiles of all the samples can be indexed using cubic fluorite structure of CeO_2 (ICDD card no. 98-010-7877) with space group $Fm\bar{3}m$. However, it is also observed that some additional weak-intensity peaks in the 2θ range of (30-55)° are present for higher compositions of the LNC content (30 and 35) in the composites (marked by *). These additional peaks correspond to the crystalline phase of LNC [Jin et al., 2018]. This specifies that even after sintering at 700^{o}C for 1.5 hours, the total amount of LNC in the nanocomposite does not convert into amorphous carbonate phase but a small fraction is retained.

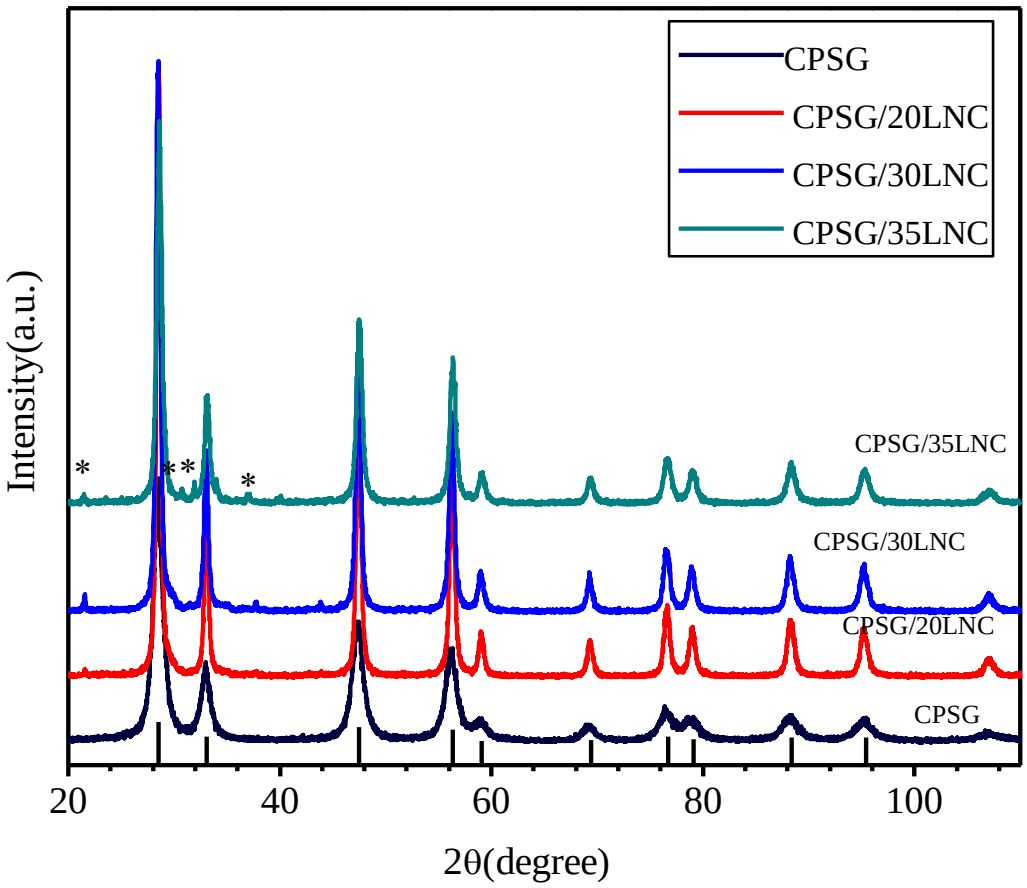

Figure 4.2 Powder X-ray diffraction patterns of the CPSG, CPSG/20LNC, CPSG/30LNC and CPSG/35LNC nanocomposites. Vertical bars at the bottom mark the reference peak positions of pure CeO_2.

Further, no other chemical reaction or extra phase formation takes place between tri-doped ceria and LNC carbonate during sintering. The average crystallite size of CPSG and CPSG-LNC nanocomposites were determined by using Debye Scherer's formula. The obtained crystallite sizes for the CPSG, CPSG/20LNC, CPSG/30LNC and CPSG/35LNC is found to be 6.37, 16.56, 17.22 and 13.56 nm respectively. Formation of liquid phase of LNC can assist in mass transport of CeO_2 grains, by liquid phase sintering mechanism, and can be responsible for the increased grain size for the nanocomposites. However, some authors have reported decrease in the grain size of ceria based alkali carbonate nanocomposites because of the hindering effect due to

amorphous phase of LNC in between CPSG grains during grain growth process [Vollath et al., 1997; Ma et al., 2010]. In liquid phase sintering, wetting characteristics of the liquid at the solid-liquid interface decides the efficiency of the mass transport process for densification and grain growth. If liquid is not wetting the solid, it will not help in grain growth mechanism as reported in some composite electrolytes [Ma. et al., 2010]. The crystallographic modifications in the structure of composite samples were analyzed by Rietveld Structure refinement using cubic space group F$m\bar{3}m$. A very good Rietveld fit for the XRD patterns of all the compositions obtained by considering fluorite structure is demonstrated in Figure 4.3 (a-d). The lattice parameter for the CPSG, CPSG/20LNC, CPSG/30LNC and CPSG/35LNC is found to be 5.4272(2), 5.4229(3), 5.4230(1) and 5.4253(8) Å respectively. Formation of composite of CPSG with LNC results into slightly decreased lattice parameter. This can be attributed to the partial incorporation of the smaller Li^{+} (0.92 Å) ions at the Ce^{4+} (0.97 Å) sites by thermal diffusion during sintering [Shannon et al., 1976].

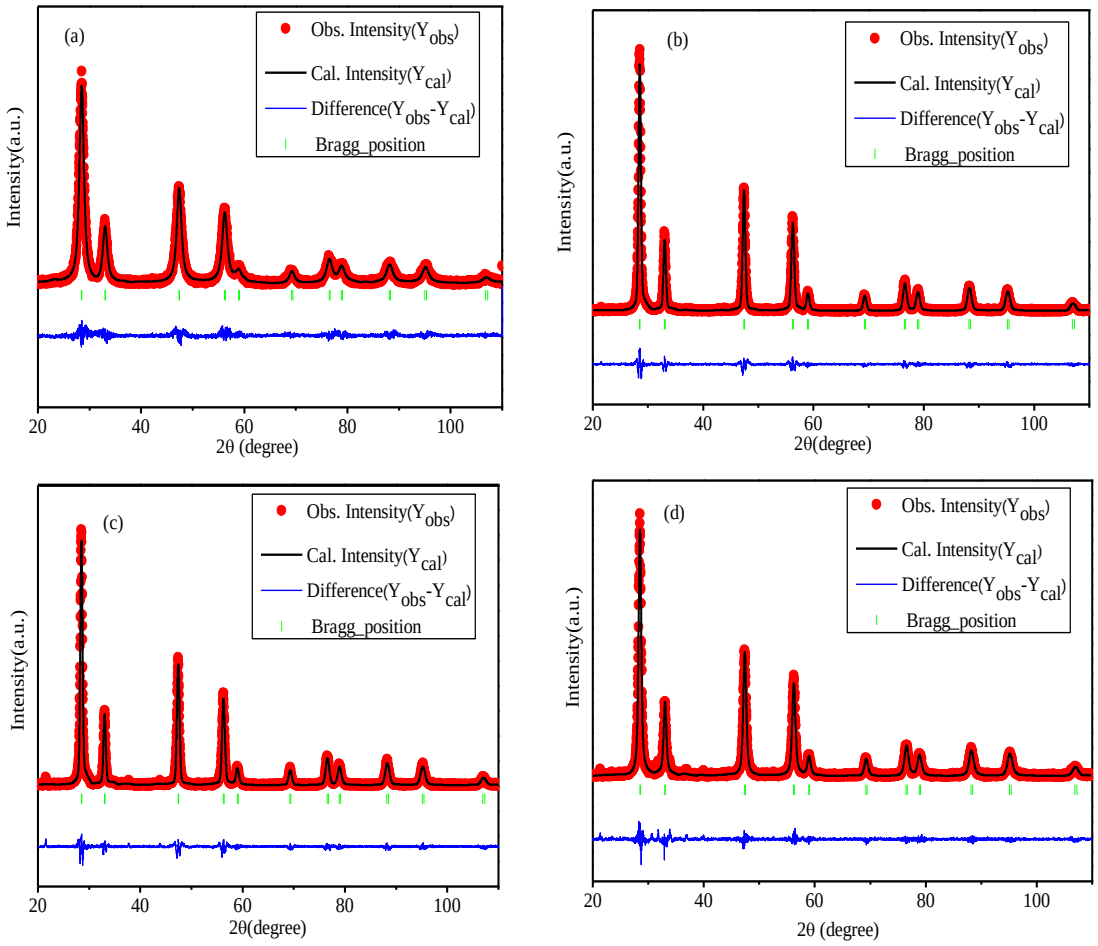

Figure 4.3 (a-d) Rietveld fits for the X-ray diffraction patterns of CPSG, CPSG/20LNC, CPSG/30LNC and CPSG/35LNC. The experimentally observed data is represented by red dots; the calculated XRD profile by black line curve overlapping on the observed data while bottom blue curve represent their difference. The positions of Bragg peaks are marked by vertical green bars.

4.3.3 Microstructure analysis

Micrograph of a cross-section of pure CPSG sample sintered in the air at 1300^{o}C for 4h is shown in Figure 4.4a, along with the micrographs of CPSG/LNC nanocomposites, sintered in air at 700^{o}C for 1.5 h (Figures 4.4 (b-d)). As illustrated in Figure 4.4a, the SEM image of pure CPSG is dense having regions of homogenously distributed spherical morphology of nanocrystalline grains. As can be seen from the

Figure 4.4(b-d), for the nanocomposite samples, the regular-sized CPSG grains are uniformly packed in the percolated network of molten carbonate phase, which appears as a continuous phase. The CPSG/LNC nanocomposites with higher amounts of carbonates could be structurally observed as continuously distributed composite particles of two constituent mixture consisting of uniform CPSG/LNC nanocomposite particles along with quasi-uniform amorphous LNC phase [Li et al., 2016]. The CPSG/20LNC and CPSG/35LNC composite samples represent the needle-like columnar structure, as represented in Figure 4.4b and 4.4d. The grain growth characteristics of the CPSG have been altered in the presence of molten LNC phase leading to the columnar structure of the grains. The incorporated carbonate phase appears to stuck the CPSG/LNC nanocomposite phases to develop a structure of non-compactly-bound binary carbonates phase. Figure 4.5 shows the elemental mapping for CPSG/35LNC, and all the elements (Ce, Pr, Gd, Sm, Na, C) are observed to be present and distributed homogeneously throughout the sample. It is already well-known that low atomic number Li cannot be identified by EDS.

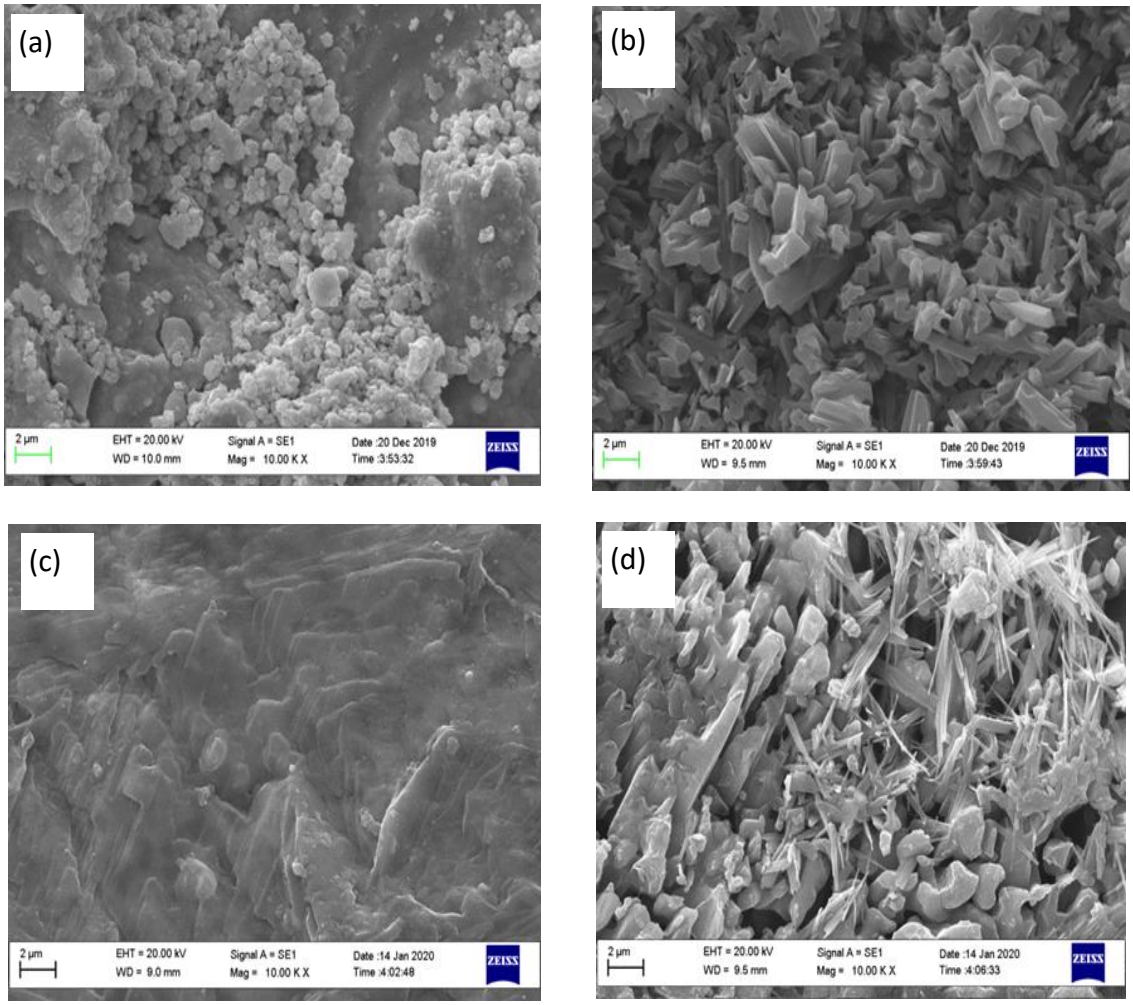

Figure 4.4 (a-d) SEM images of the of CPSG, CPSG/20LNC, CPSG/30LNC and CPSG/35LNC nanocomposite electrolytes

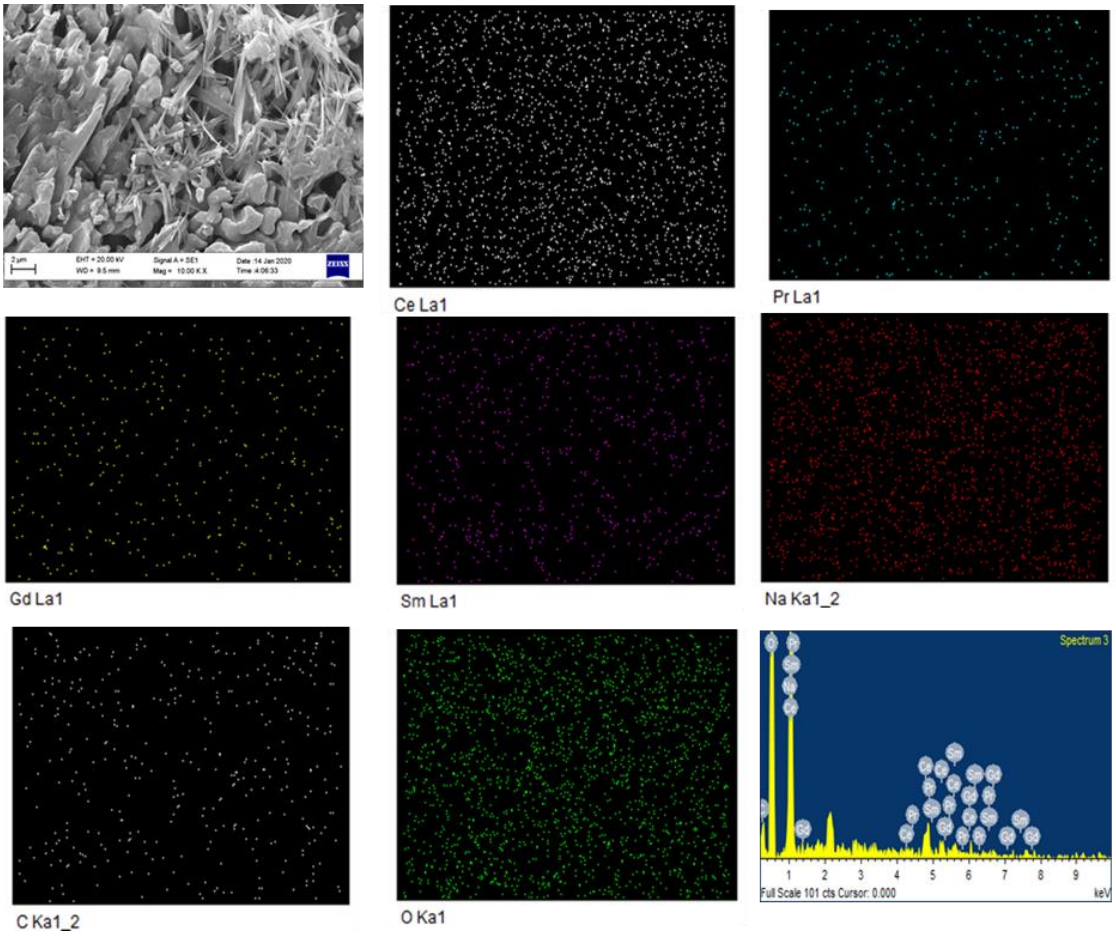

Figure 4.5 Elemental mapping of CPSG/35LNC nanocomposite electrolyte.

4.3.4 TEM analysis

Figure 4.6 illustrates the TEM images and selected-area electron diffraction (SAED) patterns of the CPSG /35LNC nanocomposite. The micrographs shown in Figure 4.6a and 4.6b clearly reveal the occurrence of secondary amorphous LNC layer (shell) over the well crystalline CPSG nano particles with the core-shell structure. The lattice planes in the amorphous shell regions are missing while they are clearly seen for the core region as shown in Figure 4.6b. The sequence of rings observed in the SAED pattern can be well matched with reported diffraction peaks of CeO_2, confirming the polycrystalline nature of triple doped ceria nanopowder. The CPSG nano-particles having rectangular-shaped crystals, and the inter-planer distance ~0.271 nm of the crystal lattice fringes corresponding to the (200) planes are also presented in Figure 4.6c

[Ortega et al., 2008]. The nonappearance of extra SAED pattern rings due to LN carbonates reveals that they are primarily in the amorphous nature. The previously reported results on typical ceria-carbonates nanocomposites are well in agreement with the present core-shell structure of our samples [Kumar et al., 2019]. Figure 4.6d demonstrates the histogram with Gaussian distribution of the crystallite size with majority of grains having sizes around 10 to 12 nm.

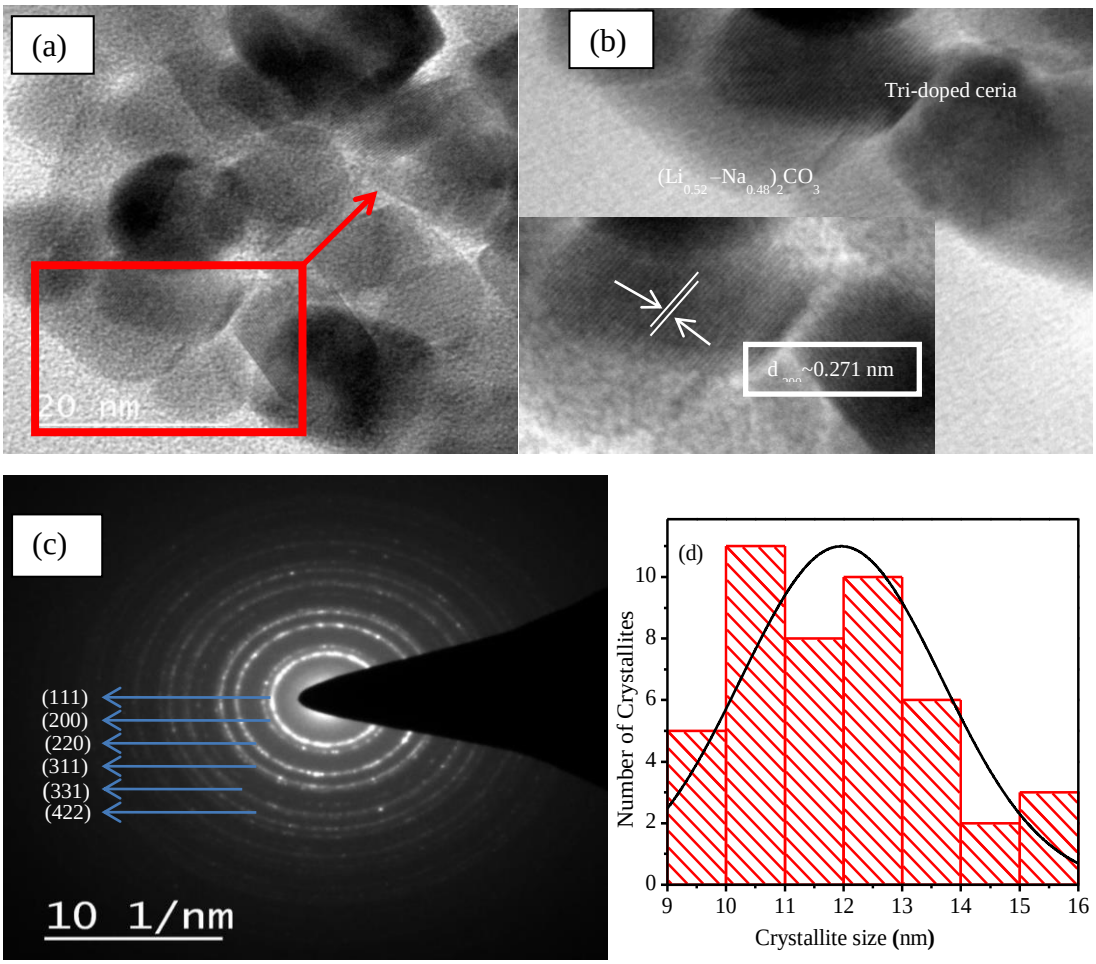

Figure 4.6(a) TEM images of CPSG/35LNC with core-shell morphology (b) high resolution TEM image of CPSG/35LNC, (c) SAED pattern of CPSG/35LNC sample (d) histogram with Gaussian distribution of crystallite size of CPSG/35LNC sample.

4.3.5 Thermal expansion behaviour

Figure 4.7b presents the thermal expansion curve of CPSG/35LNC composite determined in the temperature range (30-700°C) using high temperature XRD (HT-XRD) data as shown in Figure 4.7a. On increasing temperature, no any phase change or formation of secondary phases is observed except the appearance of a small peak of alkali carbonate at temperature 700°C. From Figure 4.7b, It is observed that the curve presents nonlinear behavior with an inflection point about the temperature range 450°C to 500°C. The phase transition from the solid to the softening phase of alkali carbonates is ascribed by inflection point about 450°C. The thermal expansion curve becomes again linear owing to the molten carbonates fill in the interspaces of CPSG grains generating a continuous path around 500°C. Coefficient of thermal expansion (CTE) was determined from expansion curve by using following formula:

$$CTE = \frac{L-L_o/L_o}{T-T_o} \qquad \text{Eq.4.1}$$

where symbols are final lattice parameter (L), the initial lattice parameter (L_0), initial temperature (T_0), and terminal temperature (T) for the solid electrolyte. The binary carbonate phase melts and forms a continuous path via filling the interspaces around 500°C which is responsible for the slightly higher value of CTE (16.7×10^{-6}) of the composite as compared to the pure CPSG sample reported by earlier authors [Venkataramana et al., 2017]. As can be seen from Fig.4.7b, the observed thermal expansion of the prepared composite electrolyte for the entire temperature range is well within the acceptable limit for the SOFC applications.

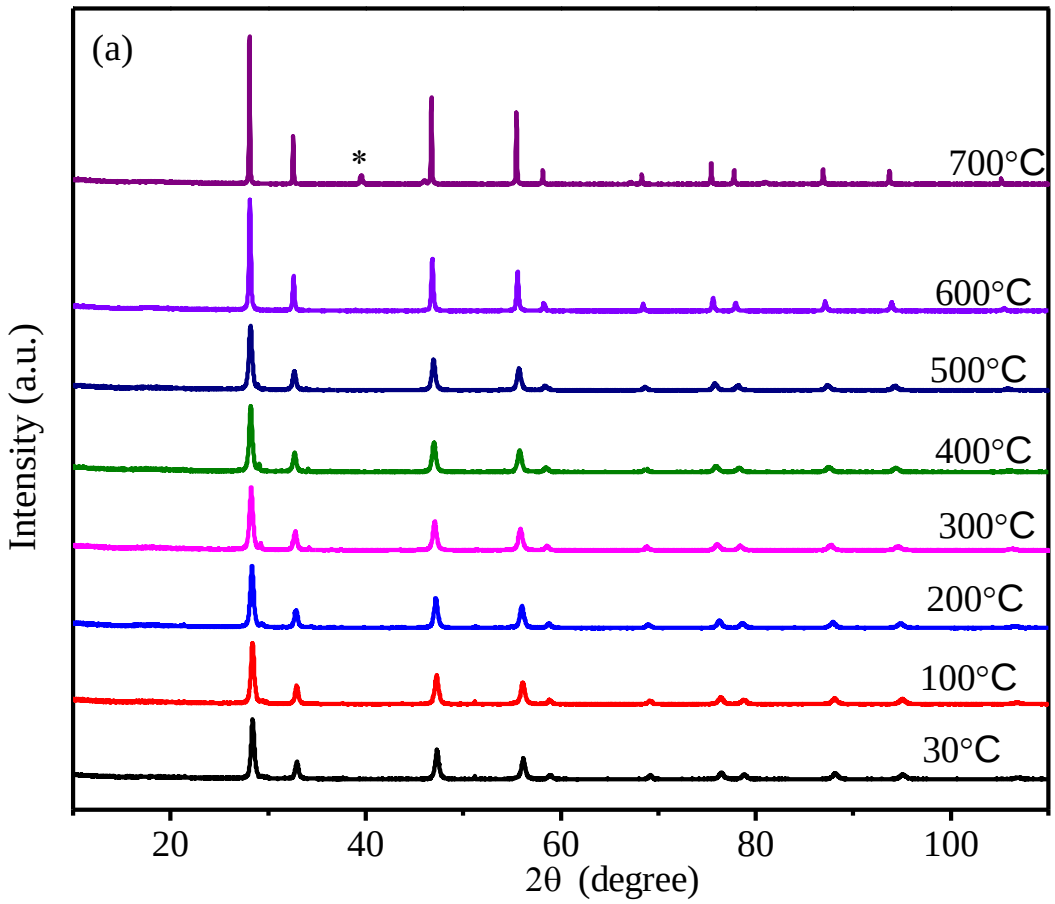

Figure 4.7 (a) Evolution of XRD patterns with temperature for CPSG/35LNC solid electrolyte

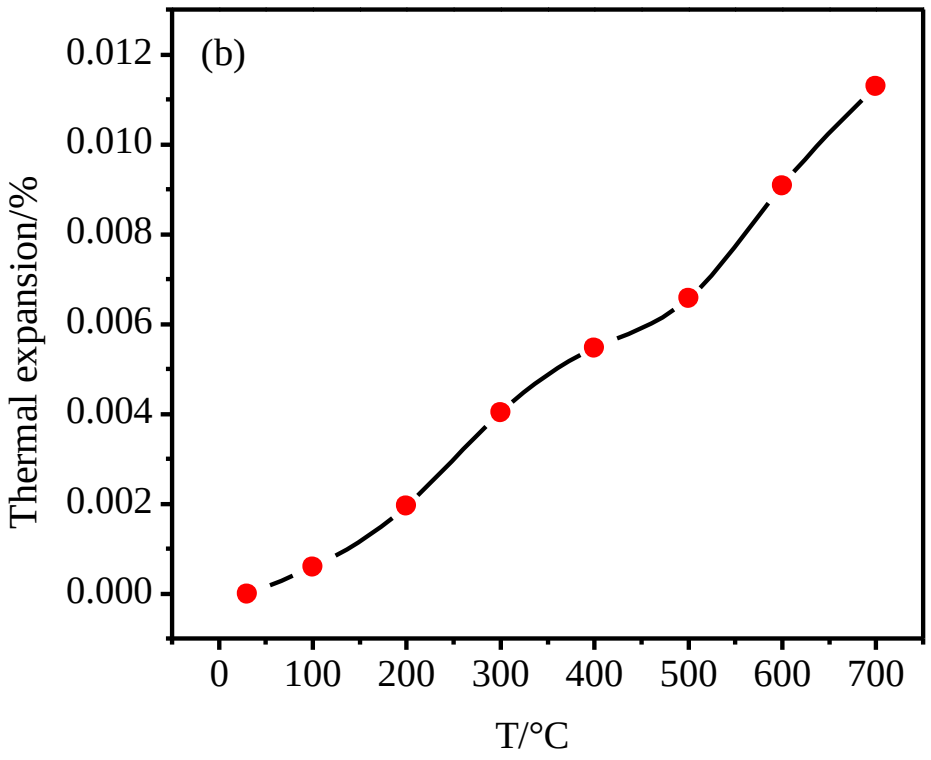

Figure 4.7 (b) Thermal expansion plot of CPSG/35LNC solid electrolyte

4.3.6 Dielectric loss behaviour

The dielectric tangent loss for CPSG, CPSG/LNC composites measured at some selected temperatures in the frequency range (20 Hz to 5 MHz) are presented in Figure 4.8(a-d). For pure CPSG, the existence of two types of dielectric relaxation mechanisms were confirmed by the well resolved peaks in the plot (Figure 4.8a) which correspond to the involvement of the grain boundaries and grains in the polarization processes. The grain boundary dielectric loss peak appears over the frequency range (100-10^4 Hz) and as measuring temperature increases, the relaxation peak shifts in the direction of higher frequency region. Similarly, the loss peak corresponding to the grain contribution is evident above 10^4 Hz that moves towards higher frequency side and at very high temperatures, it exceeds measuring frequency range of our instrument. With increasing temperature, the movement of the thermally activated ion charge carriers are enhanced and at higher frequency side, hopping charge carrier ions begin to relax thus the loss

peak is moving at higher frequency region. The dielectric loss having high peak value is directly related to relaxation process occurring because of availability of dipoles and mobility of free charge carriers [Ahmad et al., 2012]. As temperature rises above 400°C, the relaxation peaks disappear having similar relaxation constant for grain boundaries and grains.

In contrast to pure CPSG, all the composite samples confirm a single relaxation peak which comes from the existence of space-charge/interfacial polarization near the grain boundaries in the low frequency region [Iguchi et al., 1991; Younas et al., 2011; Pradhan et al., 2009]. Figures 4.8 (b,c,d) reveal that the intensity of relaxation peak of nanocomposite samples get suppressed at higher frequency side with increase in the temperature which is because of the creation of the interfaces region between CPSG and LNC phases because of local softening of the carbonate phase. It is worthy to notice here that the intensity of relaxation peaks of CPSG/LNC composite electrolytes is significantly higher than CPSG which may be due to the formation of large interfacial region in grain boundary regions with higher amount of mobile defects in space charge layer. In addition, near melting transition temperature, a sharp relaxational peak at higher frequency is present due to the multi-ion conduction. This results into long-range conduction mechanism near the interface region where O^{2-}, H^{+}, CO_3^{2-}, and alkali ions (Na^{+}, Li^{+}) exist as charge carrying ions.

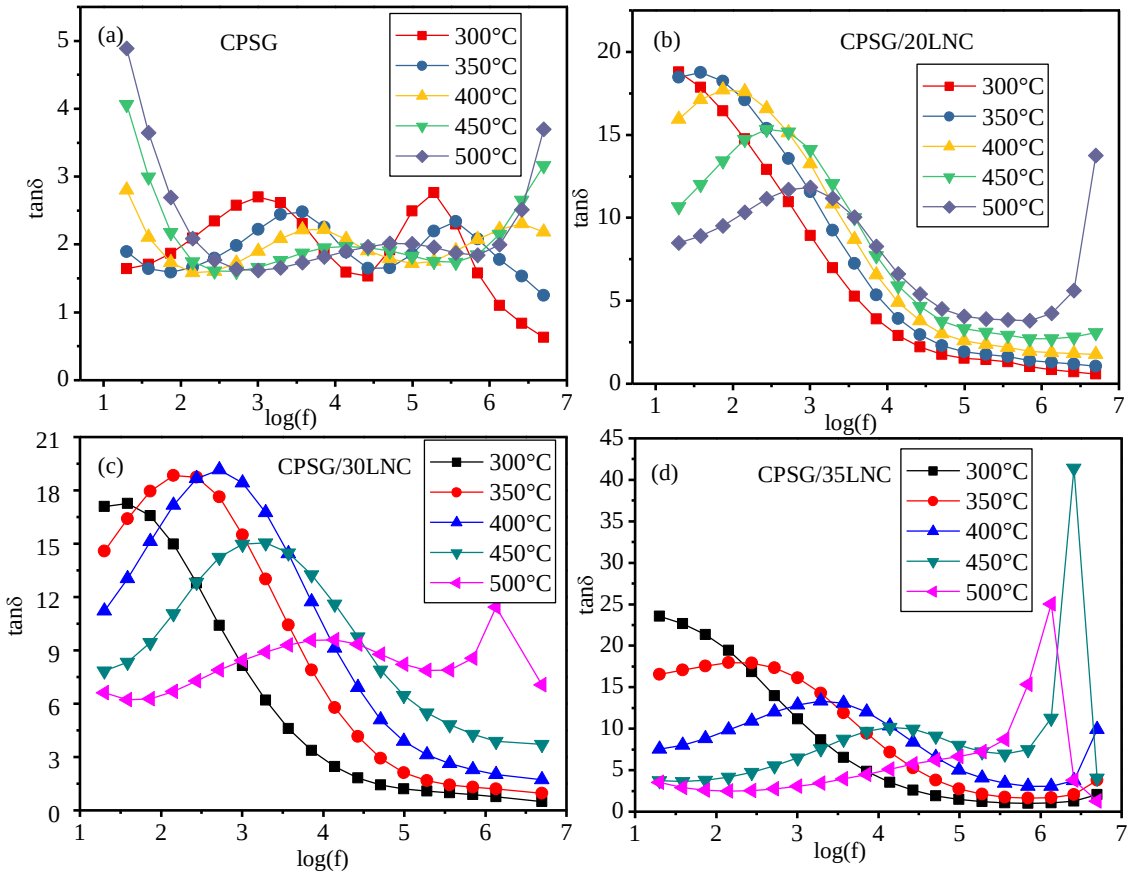

Figure 4.8 Plots of frequency dependent dielectric tangent loss for CPSG, CPSG/20LNC, CPSG/30LNC and CPSG/35LNC nanocomposite electrolytes at various temperatures.

4.3.7 ac conductivity analysis

A prevailing role of binary carbonate salt on ion-transport mechanism of triple doped ceria electrolytes composites can be inferred from the study of the ac conductivity (σ_{ac}) spectra and relaxation phenomenon. Figures 4.9 (a-d) present the variation of ac conductivity spectra as a function of frequency at a gap of 10 °C in the range of 300-500°C (increasing temperature from bottom to top curve), which can be fitted with Jonscher's power law specified by Eq.4.2.

$$\sigma(\omega) = \sigma_{dc} + A\omega^{n} \qquad \text{Eq.4.2}$$

Where $\sigma(\omega)$ is the frequency dependent total conductivity, 'σ_{dc}' is conductivity associated to dc conduction, 'A' is temperature dependent pre-factor and 'n' is dimensionless frequency exponent whose value lies between 0 and 1 [Zheng et al., 2013; Yang et al., 2010; Pradhan et al., 2012]. Figure 4.9a depicts the increasing nature of the conductivity with increasing frequency, which is caused by thermally activated hopping of oxygen ions. Figure 4.9(b-d) plots consist of a lower frequency DC plateau region, and high frequency side ascribes frequency dispersion region for the entire temperatures, which can be elucidated via the jump relaxation model (JRM) [Jonscher et al., 1999; Jonscher et al., 1977; Ortega et al., 2008]. According to JRM, lower frequency region corresponding to dc conductivity arises owing to successful hopping of ion from a vacant site to neighboring site which relates to the uncorrelated random long range motion of ions. As frequency increases, a hop of central ion to its native neighboring vacant site get started to become stable at the new position of jumped ion. The jumped ions can relax in two different kind of opposing ways. The charge ions may jump back to its original site (unsuccessful hop) which facilitate the partially relax arrangement of jumped ions or it can also become relax and stay in neighboring site (successful hop). The dispersion region arises due to decreasing of the fraction of successful hopping to unsuccessful hopping in association with the relaxation motion of ions. With addition of binary LN carbonate (Figure 4.9), the interface region is created between ceria and carbonates which effectively enhance the localized ions. Therefore, the dispersive region disappears owing to the increase of long-range hopping of localized charge carriers. Figure 4.9 clearly show that the conductivity strongly depends on concentration of binary LN carbonate in CPSG triple doped ceria electrolyte. However, the tendency changes after 30wt% LNC concentration, it decreases and shows dispersion in low frequency region at higher temperature due to fast ion transportation

i.e. electrode polarization(EP) [Dussan et al., 2012; Sumi et al., 2010]. To further explore more insight about the charge conduction process, comparative plots of exponent (n) are shown in Figure 4.10 for various compositions of CPSG/LNC nanocomposite electrolytes. The temperature variation of 'n' provides information, to identify the appropriate hopping conduction mechanism, concerned for ac conductivity, in course of level of interaction between free ions with neighbouring lattices. In present case, it suggests the level of interaction between the mobile ion charges and the amorphous percolated network of the LN carbonates. It is apparent from the Figure 4.10 that the exponent increases with temperature for pure CPSG sample. Thus for the measured temperature range, small polaron conduction (SPC) model is the most appropriate mechanism to elucidate the ac conduction behavior for this system [Sumi et al., 2010]. The SPC mechanism is a thermally stimulated one. For composite samples, with the introduction of LN carbonate in CPSG, the value of 'n' first increases up to 300°C but start decreasing when temperature exceeds beyond 300°C, owing to the large polaron formation caused by trapping of the charge carriers in the potential well due to interfacial regions. These polaronic states are not possibly thermally associated. Moreover, a large polaron can be generated via the residual carriers on account of the interaction through the positive charge ions in the lattice [Sumi et al.,2010].

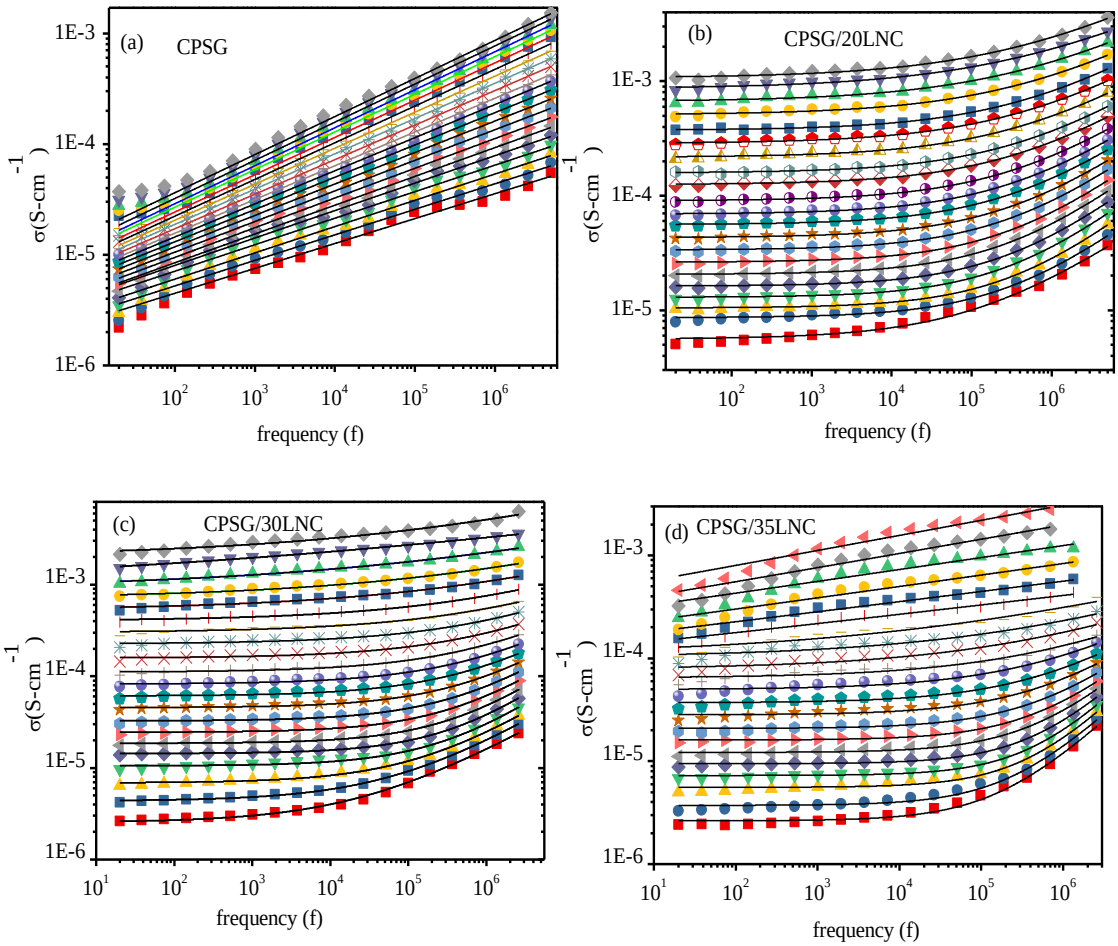

Figure 4.9 The frequency variation of complex ac conductivity for CPSG, CPSG/20LNC, CPSG/30LNC and CPSG/35LNC nanocomposite electrolytes at various temperatures in the range of 300-500°C at an interval of 10 °C (increasing temperature from bottom to top curve).

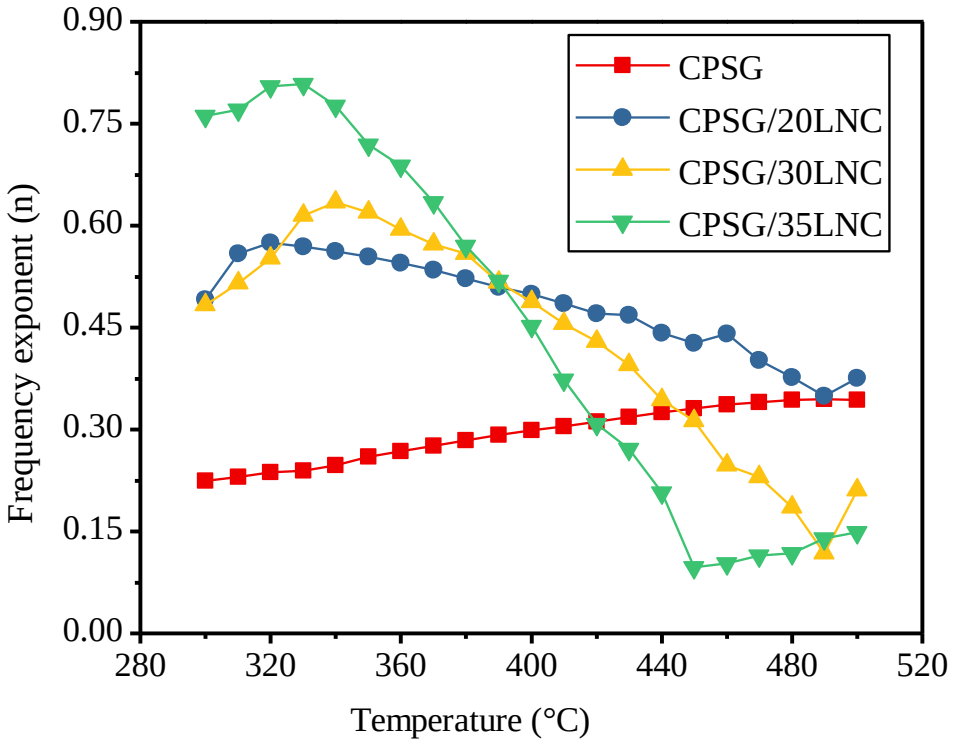

Figure 4.10 The temperature variation of frequency exponent (n) for CPSG/LNC nanocomposite samples

4.3.8 Impedance analysis

To further explore the interfacial effect on ionic conductivity of CPSG/LNC nanocomposites, the typical ac impedance plots for the sintered pellets of all electrolyte compositions were carried out in the temperature range of 200 to 650 °C in air. As shown in Figure 4.11a and 4.11b, the Nyquist plots for composite electrolytes measured under air at the temperatures 350 and 550°C reveal, one semicircle arc at high frequency region corresponding to the response of bulk composite along with one low frequency tail ascribed to resistance arising due to electrode/electrolyte interface as well as mass diffusion process. It is observed from the plots of impedance spectra of composite electrolytes that distinct arc component from the grain boundaries is not present, which is supposed to begin from the strong interactions among the CPSG crystallites and LN

carbonate phases. At 550°C, Nyquist plots reveal the sudden reduction in the electrolyte conduction resistance because of superionic phase transition at the interface phase, as a result of molten form of the LN carbonate phase. A long tail at high frequency range is ascribed to inductance effect due to contact wires. It can be inferred from these Nyquist plots that conduction processes are governed through vacancy conduction. Below transition temperature, the solidified carbonate will reduce the conductivity via blocking the path of vacancy conduction. Alternatively, above the melting transition temperature, the molten alkali carbonates provide fast ions transport channel as well as conduction of multi-ions (O^{2-}, CO_3^{2-}, H^+, Na^+, Li^+) which greatly improve the conductivity. The CPSG/35LNC solid electrolyte exhibited the lowest resistance over entire temperature range. The values of total resistance were acquired from the best simulated fitted results of the Nyquist plots via Z-Simpwin program and the equivalent circuit was drawn including a R_1 resistance and two parallel electric circuit of R_2-CPE_1 and R_3-CPE_2 as shown in Figures 4.11c and 4.11d. Due to microstructural inhomogeneities of materials, the simple capacitor is not enough to fit the experimental data of impedance measurement. The values of elements of equivalent circuit for sample CPSG/35LNC at 350 °C and 550 °C are given in Table 4.1. The total conductivities (σ) of the all the samples were estimated and listed in Table 4.2 by using the expression, $\sigma = T/AR$, where T, A and R are the pellet thickness, surface area and resistance of pellet sample respectively. The total conductivity plots for CPSG/LNC composite electrolytes in the temperature range 200 to 650°C for various LN carbonate concentration in nanocomposites are shown in Figure 4.12. With increasing the LN carbonate content in tri-doped ceria sample CPSG, the ionic conductivity of the composites is improved [Uthayakumar et al., 2016]. In the present study, the samples having higher content of carbonates (>35 wt %) were deformed after sintering because of huge volume of the

liquid formed, thus measurements were not executed. The sudden increase in conductivity above 450°C is due to superionic conduction transition at interface of composites. In case of pure CPSG, the migration of oxide ions through oxygen vacancies is responsible for electrical conductivity. After addition of LN carbonate in to CPSG, ceria-carbonate interface forms a space charge layer (SCL), which favorably control the defect concentration near the interface and transport properties as reported earlier in similar system [Ricca et al., 2018]. Sato et al have established that an angstrom-size SCL assists contact amongst grain-to-grain for ions transportation in Li-doped GDC nano samples [Sato et al., 2015]. In the present investigations of CPSG/LNC nanocomposites, the CPSG crystallites are put in a nutshell of thin amorphous carbonate interface layer, as depicted in TEM images. From this perspective, it is predicted that oxygen ions transportation takes place within CPSG grains and then gets transferred to another grain via the amorphous interface layer of alkali carbonate while other group of ions will transfer via an amorphous layer of carbonates in a thermally activated atmosphere [Kumar et al., 2019].

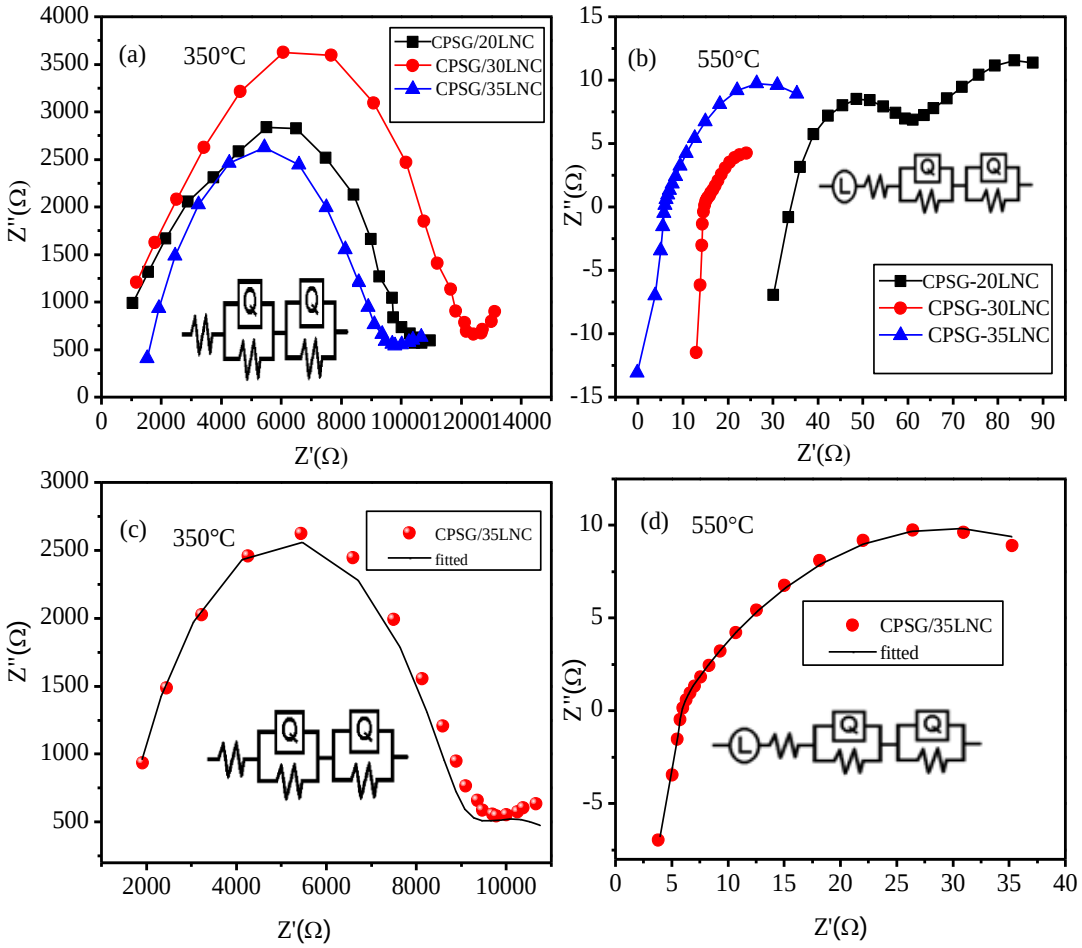

Figure 4.11 (a-b) ac impedance spectra of CPSG/20LNC, CPSG/30LNC and CPSG/35LNC nanocomposite electrolytes at 350^{o}C and 550^{o}C temperatures. (c-d) Typical equivalent electrical circuits for impedance plot of CPSG/35LNC at 350 ^{o}C and 550 ^{o}C temperatures.

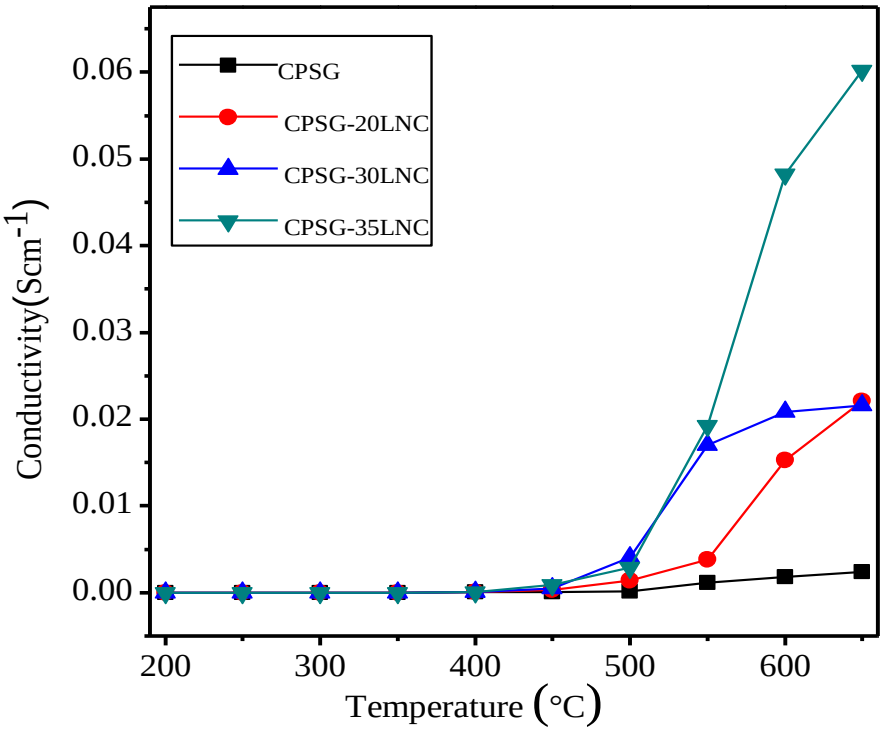

Figure 4.12 Temperature dependence of Ionic conductivity of CPSG, CPSG/20LNC, CPSG/30LNC and CPSG/35LNC nanocomposite electrolytes in the temperature range 200 to 650°C.

Table 4.1 Values of elements of equivalent circuit for CPSG/35LNC sample at 350 °C and 550 °C

Sample	Temperature	L(H)	R_1 (Ω)	Q^{-Y0} ($\Omega\ s^{-n}$)	Q^{-n}	R_2 (Ω)	Q^{-Y0} ($\Omega\ s^{-n}$)	Q^{-n}	R_3 (Ω)	$\chi 2$
CPSG/35LNC	350ºC	------	132	2.915E-9	0.76	7292	2.993E-5	0.3705	3350	2.708E-03
CPSG/35LNC	550ºC	5.736E-7	5.805	8.366E-5	0.87	0.727	8.97E-4	0.5476	42.49	5.037E-04

Table 4.2 Total ionic conductivity for CPSG, CPSG/20LNC, CPSG/30LNC and CPSG/35LNC nanocomposite electrolytes

Sl. No.	Sample	Conductivity (S/cm)			
		500°C	550°C	600°C	650°C
1	CPSG	1.76×10^{-4}	1.10×10^{-3}	1.85×10^{-3}	2.36×10^{-3}
2	CPSG/20LNC	1.37×10^{-3}	3.81×10^{-3}	1.52×10^{-2}	2.21×10^{-2}
3	CPSG/30LNC	4.04×10^{-3}	1.70×10^{-2}	2.09×10^{-2}	2.15×10^{-2}
4	CPSG/35LNC	2.85×10^{-3}	1.92×10^{-2}	4.82×10^{-2}	6.02×10^{-2}

4.3.9 Dielectric permittivity

The frequency dependence of the real part of the complex dielectric permittivity ($\varepsilon^{/}$) at various temperatures for CPSG/LNC nanocomposite samples is shown in Figure 4.13(a-d). For CPSG sample (Figure 4.13a), it is clearly seen that $\varepsilon^{/}$ exhibits high value of dielectric permittivity in the low frequency region due to polarization of oxygen ions and defect charge carriers at electrode-electrolyte interface. The other CPSG/LNC compositions show similar behavior with higher values of $\varepsilon^{/}$ due to enhanced SCL polarization at hetero-interface between ceria and alkali carbonates phase [Anirban et al., 2016]. The value of dielectric permittivity diminishes rapidly with increasing frequency, which can be elucidated by the difficulties encountered by charge carriers in following the alteration of applied electric field beyond a certain frequency due to their larger sizes. At higher frequencies also, the dielectric permittivity shows dispersive nature which may be due to thermally activated hopping mechanism, leading to disappearance of saturation region [Sumi et al., 2010, Wang et al., 2017].

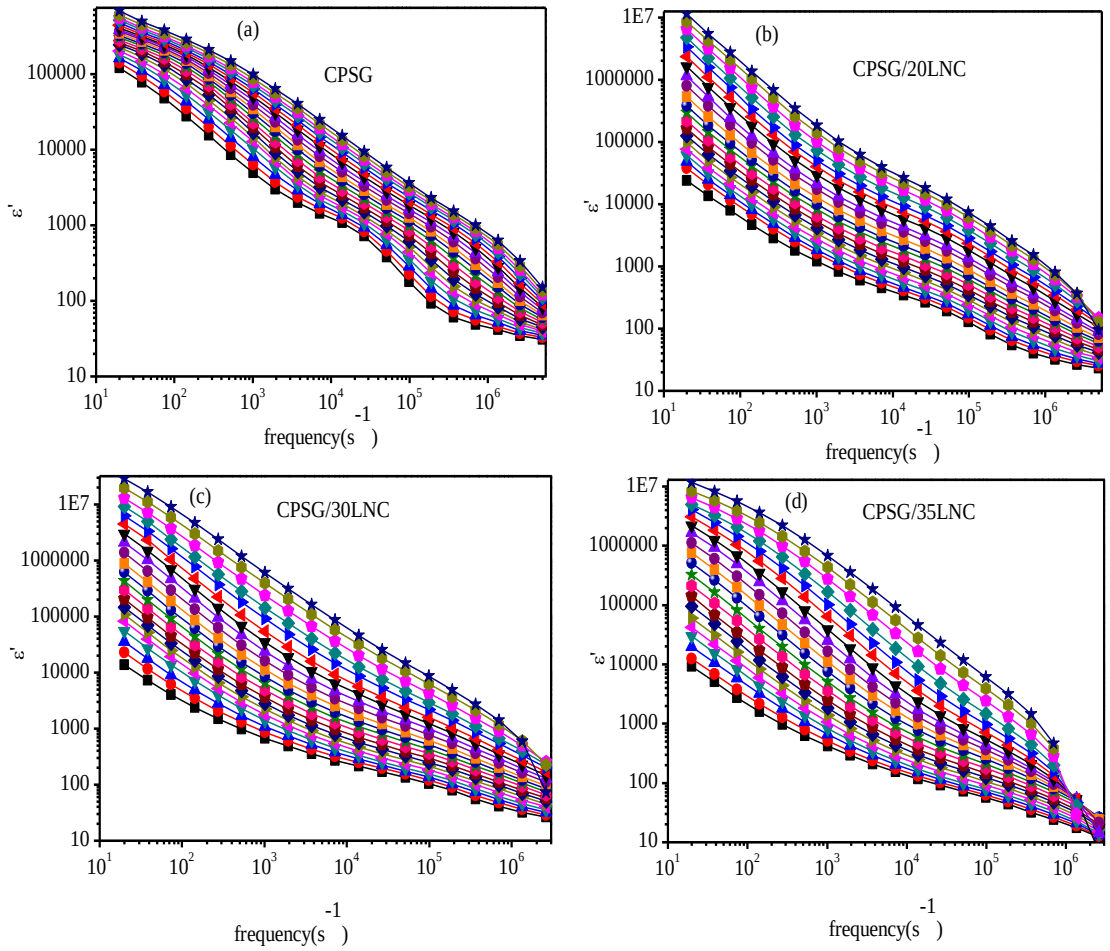

Figure 4.13 Frequency variation of real part of dielectric permittivity for CPSG, CPSG/20LNC, CPSG/30LNC and CPSG/35LNC nanocomposite electrolytes in the temperature range of 300-500 °C at an interval of 10 °C (increasing temperature from bottom to top curve).

4.4 Conclusions

A detailed study of the structural, electrical, ionic conductivity and ion charge transport properties of $Ce_{0.76}Pr_{0.08}Sm_{0.08}Gd_{0.08}O_{2-\delta}/(Li_{0.52}Na_{0.48})_2CO_3$ nanocomposite electrolytes with various compositions, have been done. The role of the alkali carbonates content in improving the ionic conductivity of nanocomposites is investigated. The XRD analyses of the nanocomposites confirm the CeO_2 like single

phase formation of CPSG with amorphous phase of LN carbonates. The average crystallite sizes of the nanocomposites are enhanced than the pure CPSG due to liquid phase sintering. Microstructural characterization of the nanocomposites by SEM and TEM reveal uniform distribution of both phases with ceria grains packed within the percolated network of amorphous molten alkali carbonate phase. Significantly improved ionic conductivity is obtained in all the nanocomposite samples due to interfacial conduction phenomenon. The core-shell like structural morphology facilitates stimulated space charge layer as a result of strong columbic interactions among the tri-doped ceria and amorphous phase of alkali carbonates. The space charge layers provide the extra path and direct the mobile charge carrier groups to their preferred conduction paths in the composite electrolytes. The CPSG/35LNC composition, gives maximum conductivity of 6.02×10^{-2} S-cm^{-1} at 650 °C, which is significantly higher than the pure CPSG electrolyte. These results establish that, a nanocomposite of an advanced alkaline carbonate incorporated in a ceria based electrolyte, in place of one or multiple rare earth ions doped ceria, can provide a low-priced solid oxide electrolyte material for low/intermediate temperature regions.